Available online at www.sciencedirect.com
ScienceDirect
Journal of Sound and Vibration 314 (2008) 783–802
JOURNAL OF SOUND AND VIBRATION
www.elsevier.com/locate/jsvi

Nonlinear vibration of cable-stiffened pantographic deployable structures

G.E.B. Tan[a], S. Pellegrino[b,*]

[a]DSO National Laboratories, 20 Science Park Drive, Singapore 118230, Singapore
[b]Graduate Aeronautical Laboratories, California Institute of Technology, 1200 E. California Blvd, MC 301-46, Pasadena, CA 91125, USA

Received 15 September 2006; received in revised form 8 January 2008; accepted 8 January 2008
Handling Editor: M. P. Cartmell
Available online 3 March 2008

Abstract

Cable-stiffened deployable pantographic structures are fully prestressed at the end of deployment. Indirect effects of this state of prestress are increased stiffness and friction at the end joints of the pantograph rods, and increased cable damping. Both effects are a function of the prestress level in each particular component, are amplitude dependent and frequency dependent, and can be characterized using the restoring force identification method after carrying out component level tests. For a particular model structure it is shown that the resonant frequencies of its first 4 modes tend to decrease when the excitation amplitude is increased, whereas the variation in the modal damping is non-monotonic. A nonlinear dynamic model of this structure is set-up, which accounts for the effects of joint preload and passive cable pretension via equivalent stiffness and damping coefficients. This model predicts accurately the resonant frequencies of the first 4 modes. It also predicts modal damping to good accuracy, provided that unmodelled degrees-of-freedom, such as joint rocking, are not excited.

1. Introduction and background

Deployable space structures are a special type of structure designed for compact stowage and automatic expansion in orbit; their current applications include booms, solar arrays, and antennae. Different structural concepts have been developed, which address in different ways the conflicting requirements of effective packaging and efficient, reliable structural behaviour [1,2]. A characteristic common to practically all of these structures is that they exhibit nonlinear behaviour, particularly under dynamic excitation, which makes their response difficult to predict. Thus, there have been many instances of unexpected dynamic coupling between the flexible modes of a deployable structure and the attitude control of the spacecraft supporting it. The next generation of deployable structures for, e.g. earth-observation radar and space telescopes, will be subject to stringent operating requirements [3,4] and active shape and vibration control are expected to play an increasing role in achieving the required accuracy. Most control techniques developed for large flexible space

*Corresponding author. Tel.: +1 626 395 4764; fax: +1 626 449 2677.
E-mail address: sergiop@caltech.edu (S. Pellegrino).

0022-460X/$ - see front matter © 2008 Elsevier Ltd. All rights reserved.
doi:10.1016/j.jsv.2008.01.022

structures require an accurate model of the structure. In particular, good estimates of structural damping are required, because the level of passive damping directly influences the robustness and stability of the active control, which in turn affects mission performance.

The aim of this paper is to investigate the effects of component nonlinearities on the vibration of cable-stiffened deployable pantographic structures [5,6]. These structures consist of a *pantograph*, formed by pairs of rods connected in the middle by means of scissor joints and at the ends by revolute joints. The pantograph behaves as a backbone with a single internal degree-of-freedom, which is deployed by a small number of *active cables*, running over pulleys attached to the revolute joints, and connected at one end to motor-driven pulleys. In the fully deployed configuration the stiffness of the pantograph is increased by a series of *passive cables* becoming taut and prestressed. The particular structure that will be investigated in this paper is the Triangular Pantographic Mast, shown in Fig. 1 and described in detail in Ref. [5].

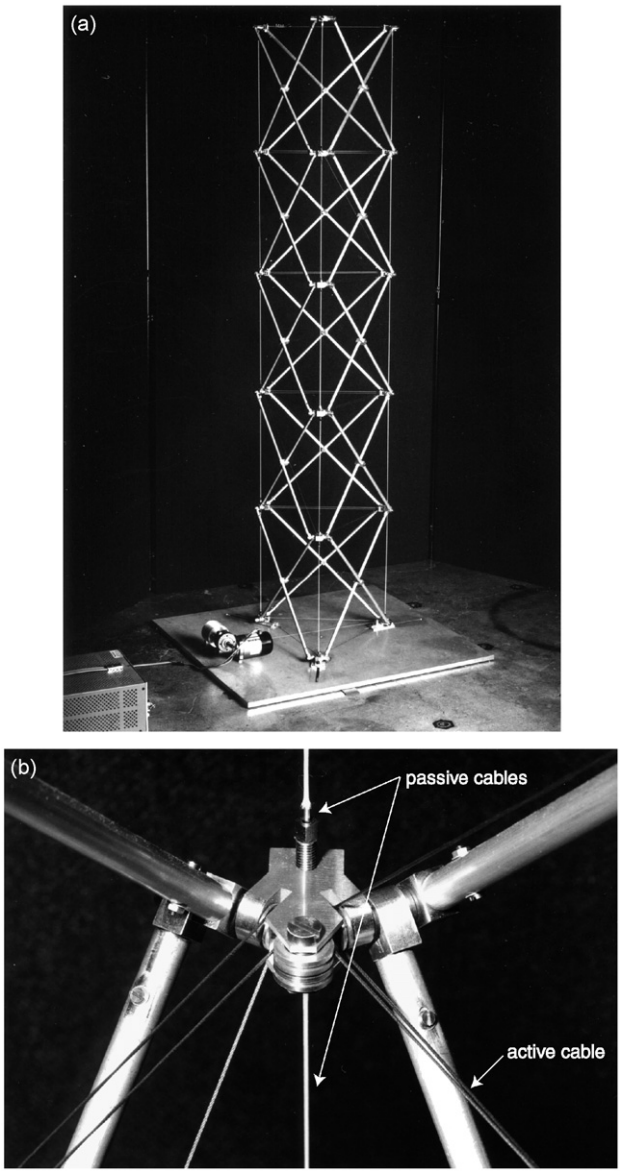

Fig. 1. Pantographic deployable structure: (a) fully deployed configuration; (b) joint detail.

It has been previously shown that structures of this type can achieve their deployed shape repeatably and with good accuracy, and also behave almost linearly under static loading. It will be shown in this paper that nonlinearities, whose effects are small under static conditions, become more important when these structures are excited dynamically. The overall effect is high modal damping, particularly for certain modes. It will be shown that the key sources of nonlinear behaviour are micro-slip in the joints and changes in damping in the cables. Both of these effects are related to the level of prestress applied to the structure by the active cable, and can be modelled analytically after carrying out component tests with specially designed apparatus. These ''local'' models are incorporated in a global dynamic model with non-proportional damping whose predictions are remarkably close to the measured behaviour of a model structure.

The technique that will be used in this paper for representing the steady-state vibration of the nonlinear components of a pantographic structure is known as describing function method [7]. In this method the transfer function of any given nonlinear element is approximated by its first harmonic. Thus, for a displacement input

$$y = A\sin\omega t, \tag{1}$$

the transfer function is approximated by

$$\tilde{F}_{\mathrm{NL}} \approx a\sin\omega t + b\cos\omega t = a\sin\psi + b\cos\psi, \tag{2}$$

where $\psi = \omega t$. Multiplying Eq. (2) by $\sin\psi$ and integrating, and repeating also for $\cos\psi$ gives

$$a = \frac{1}{\pi}\int_0^{2\pi} F_{\mathrm{NL}}\sin\psi\,\mathrm{d}\psi, \tag{3}$$

$$b = \frac{1}{\pi}\int_0^{2\pi} F_{\mathrm{NL}}\cos\psi\,\mathrm{d}\psi. \tag{4}$$

Rearranging Eq. (1)

$$\sin\omega t = \frac{y}{A} \tag{5}$$

and, differentiating

$$\cos\omega t = \frac{\dot{y}}{\omega A}. \tag{6}$$

Substituting Eqs. (5) and (6) into Eq. (2)

$$\tilde{F}_{\mathrm{NL}} \approx \frac{a}{A}y + \frac{b}{A\omega}\dot{y} = k_{\mathrm{eq}}y + c_{\mathrm{eq}}\dot{y}, \tag{7}$$

where

$$k_{\mathrm{eq}} = \frac{1}{\pi A}\int_0^{2\pi} F_{\mathrm{NL}}\sin\psi\,\mathrm{d}\psi, \tag{8}$$

$$c_{\mathrm{eq}} = \frac{1}{\pi A\omega}\int_0^{2\pi} F_{\mathrm{NL}}\cos\psi\,\mathrm{d}\psi. \tag{9}$$

The equivalent stiffness k_{eq} and the equivalent damping c_{eq} are the *describing function coefficients* of the nonlinear element.

Much research into nonlinear vibration of space structures has been carried out. Of particular relevance to the present study is the paper by Bowden and Dugundji [8], where describing functions were used to examine the effects of nonlinear joints on the overall dynamics of space structures. An analysis of a four segment beam whose joints incorporated cubic stiffening springs and linear viscous dampers, which gave rise to non-proportional damping, showed that increasing joint damping caused the resonant frequencies to increase, but only up to the point where the joints became effectively locked. Classical single-degree-of-freedom (sdof) nonlinear behaviour was observed at each resonant frequency, including non-proportional increases in

response amplitude with increasing excitation forces, resonant frequency shifts, etc. These nonlinear effects were more significant when the stiffness of the joints was low, and for modes that involved significant joint motion. The first four modes of a simple two-dimensional pantographic structure, computed using the same approach as in Bowden and Dugundji [8], show a similar variation, see Fig. 2(a), but this behaviour cannot be captured by a standard proportional damping model, Fig. 2(b). Studies by Chapman [9] and Onoda [10] of trusses with nonlinear joints have shown the potential for energy transfer from lower to higher modes.

On the experimental front, links between nonlinear joint behaviour and global dynamic response are well documented [11–13], but so far most attempts to link nonlinearities at component level with overall dynamic behaviour have had only limited success. One of the main tools for nonlinear identifications is the force state

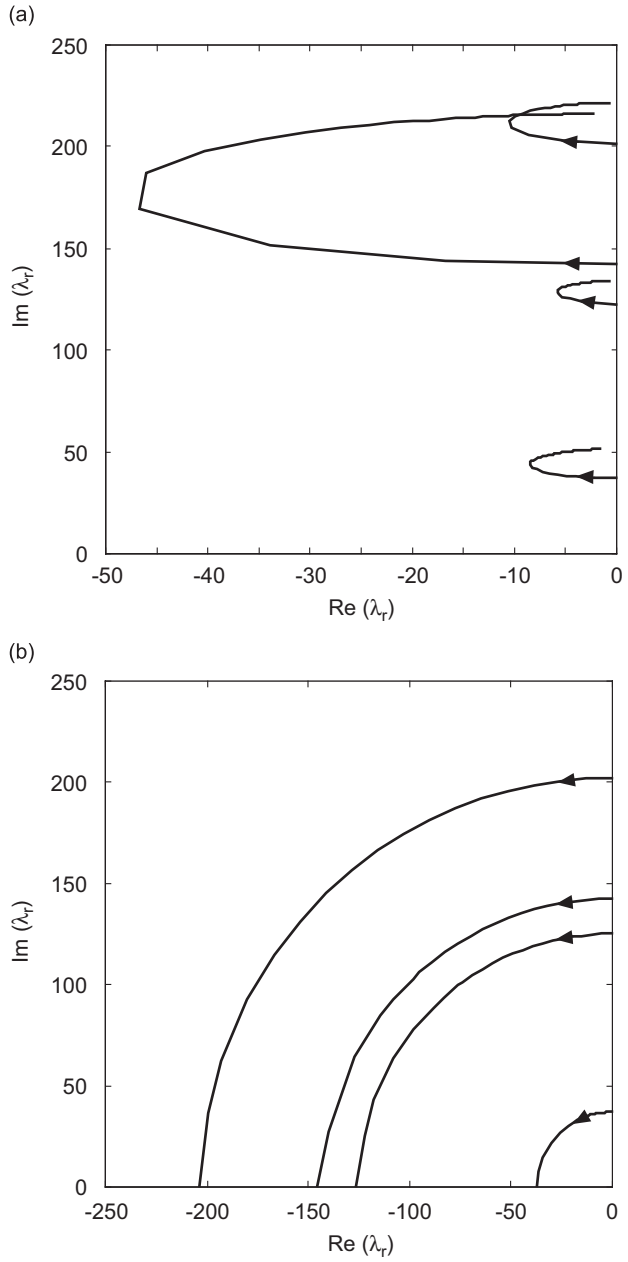

Fig. 2. Root loci for different damping models; arrows indicate the effect of increasing damping: (a) non-proportional; (b) proportional.

mapping technique [14], based on the idea that any unknown system parameter of a multi-dof system can be estimated by a least-squares fit between measured excitation forces and states of the system. In practice, one takes direct measurements of some states, e.g. velocity and acceleration of each dof together with the corresponding applied forces, at several time steps, and then obtains the remaining states by numerical integration. Consider, for example, a sdof system that, in addition to the standard linear terms, is to be modelled by including quadratic and cubic stiffness terms. The equation of motion has the form

$$m\ddot{y} + c_1\dot{y} + k_1 y + k_2 y^2 + k_3 y^3 = F, \tag{10}$$

where m, c_1, k_1, k_2, k_3 are unknown. Assume that the total number of data samples is s, the nth sample being $\ddot{y}_n$, $\dot{y}_n$, y_n, and F_n. Substituting these values into Eq. (10) gives

$$m\ddot{y}_n + c_1\dot{y}_n + k_1 y_n + k_2 y_n^2 + k_3 y_n^3 = F_n, \tag{11}$$

which is a linear equation in m, c_1, etc. Considering all samples, one obtains a system of s linear equations in five unknowns only, whose solution yields the required system parameters. See Ref. [15] for further details and an efficient solution method.

The force state mapping technique was used by Crawley and co-workers to identify a multi-bay structure that was tested both in the laboratory and in orbit, during the course of the Mid-Deck Zero Gravity Experiment. This structure consisted of interconnected deployable and erectable bays, linked by bays containing a rotary joint, and could be arranged in different configurations. Modal tests on the ground had shown softening and increased damping when the input force amplitude had been increased [16]. These effects were attributed to micro-friction in the joints of the deployable bays. In orbit these nonlinearities became more pronounced. Masters and Crawley [17] describe a sophisticated 6 dof component tester from which force state maps of the bays of the structure were derived. Nonlinear beam element models of the different types of bays were set up, leading to global models of two different configurations of the structure [18]. Predictions of the fundamental mode response of the structure generally showed similar trends to the experimental data but some tuning, in the form of linear and nonlinear participation factors, was needed to capture the effects of gravity and cable-induced pre-tensioning.

Another experiment involving both ground and on-orbit vibration experiments of a space structure was the Joint Damping Experiment [19] on a three bay cantilevered erectable truss. Ground tests showed that damping varied by up to a factor of 8 when the orientation of the truss was changed from horizontal to vertical, and a complex amplitude dependent behaviour was also observed. Orbital tests showed similar amplitude-dependent variations and a higher overall level of damping [20], which was attributed to the gravity preload in the ground tests reducing the level of micro-impacts in the joints. Attempts to characterize nonlinear behaviour in an unprestressed pinned joint using the restoring force technique [21] have shown that rebounding across any internal gaps leads to chaotic behaviour, which makes it impossible to set up a consistent force state map.

The layout of the paper is as follows. First, the deployable model structure used for the vibration experiments is described, together with the experiments which were carried out to identify its first 4 modes and the dependence of the corresponding resonant frequencies and modal damping coefficients on the excitation level. Component tests were carried out on a joint of the pantograph and on a passive cable, and in both cases the effects of different levels of preload were investigated, in order to determine the restoring force maps for these elements. Next, a dynamic model of the structure is developed, based on a linear formulation of all components of the mast with additional nonlinear, frequency and amplitude dependent terms, for the end joints of the pantograph and the passive cables. Finally, nonlinear modal predictions are obtained from the model and are compared to the measured behaviour of the structure. A discussion concludes the paper.

2. Model structure

The experiments described in this paper were conducted on a small-scale deployable pantographic mast structure specially made for this study, but similar to that described by You and Pellegrino [5]. See Fig. 1. The pantograph is made of pairs of 500 mm long Al-alloy tubes (outer diameter 9.5 mm and inner diameter 7.7 mm) connected by steel pins in the middle. The ends of the rods are connected by steel pins to end hubs, through Glacier polyamide flanged journal bearings. The end hubs are 14 mm thick Al-alloy blocks that, in

addition to providing connection points for the rods of the pantograph, house the pulleys for the active cable and also provide termination points for the passive cables, see Fig. 1(b).

The passive cables consist of Kevlar yarns covered by a Nylon sheath. They are 340 mm long, and have a nominal diameter of 0.6 mm; their axial rigidity is 16.9×10^3 N. Both ends of each cable are glued to steel terminators with either a right-hand or a left-hand thread on the outside, so that the length of all passive cables can be adjusted by turning these terminators without twisting the cable.

The mast is mounted on a 12 mm thick Al-alloy base plate: the three bottom end hub run into radial slots on this plate, set at angles of 120°. Deployment is controlled by an electric DC motor, through a 0.8 mm diameter multi-stranded steel cable. The total height of the fully deployed structure is 1.77 m and its total mass 2.05 kg. When the structure is deployed vertically upwards the active cable tension decreases from about 20 N (mast fully retracted) to about 2.5 N (end of deployment).

3. Vibration experiments

Preliminary broadband modal tests were conducted to determine the natural frequencies and mode shapes of the model structure. These were followed by detailed modal identification tests. All tests used a single shaker, bolted to a mass of up to 4 kg, held suspended by a vertical cord, and connected through a drive rod to one of the three joint hubs at the top of the mast.

Three separate sets of modal identification tests were carried out, all for the same joint, but for a different direction of excitation (radial and tangential, in a plane parallel to the base of the mast, and also longitudinal). Tri-axial acceleration measurements were taken at all 15 joints, and standard signal processing techniques were applied to calculate frequency response functions (FRFs) of mobility, i.e. velocity/force for the particular joint and direction that had been excited. See Fig. 3 for sample results. Note that multiple-input excitation had to be rejected because, due to the flexibility of the mast, nominally independent excitations became coupled through the bending stiffness of the stingers connecting the shakers to joint hubs.

The mast was tested at two different levels of active cable pretension, 24 and 33 N, and the resulting data were analysed using the polyreference identification algorithm [22]. Three global modes were identified in the range 0–100 Hz. The frequencies of these three modes are approximately 6, 35, and 63 Hz. In addition, by exciting the mast in the longitudinal direction, a fourth mode was identified at approximately 55 Hz. The corresponding mode shapes are shown in Fig. 4: modes 1 and 2 correspond to the first and second bending modes of a cantilever beam. Because the mast has three-fold symmetry if the active cable is ignored, the driving point FRFs for radial excitation are practically identical at symmetric joints, up to about 50 Hz. But

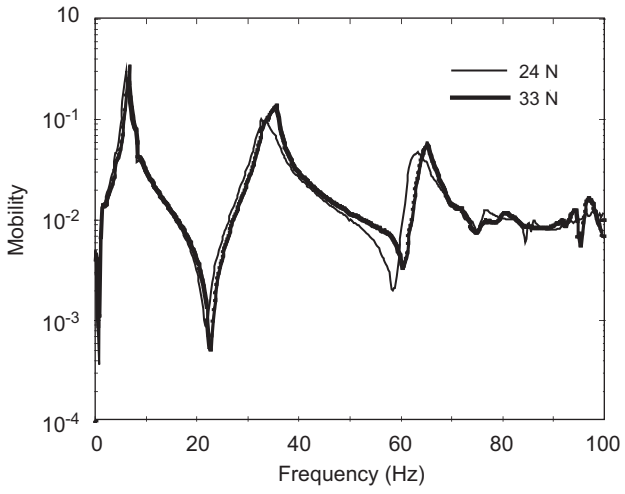

Fig. 3. FRFs for a joint at the top of the mast, excited in tangential direction, at two different values of active cable tension; both velocity and force are at the same point and in the same direction.

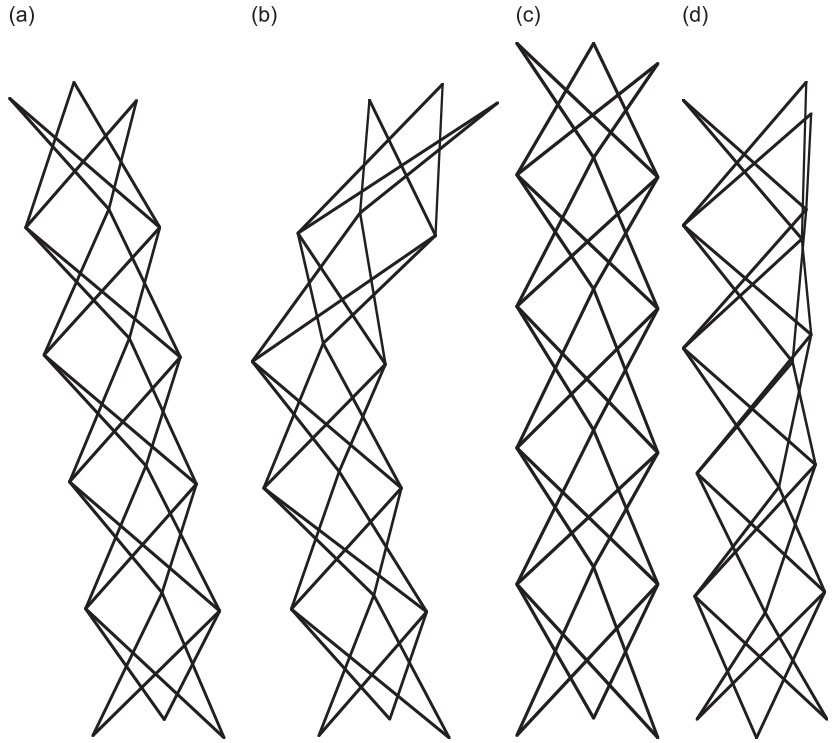

Fig. 4. Experimentally measured mode shapes: (a) mode 1; (b) mode 2; (c) mode 3; (d) mode 4.

they lose symmetry at higher frequencies, due to the combined effects of small asymmetries and the existence of several local twisting modes above this frequency.

Fig. 3 shows that the natural frequencies of the global modes shift upwards when the prestress is increased. This result indicates that increasing the active cable tension has the effect of stiffening the mast.

The broadband modal tests served the purpose of identifying the first four global modes of the mast, but also indicated that the behaviour of the mast is nonlinear. Therefore, more detailed narrow band sine sweeps tests were conducted to establish the effects of varying (i) the excitation force amplitude, (ii) the active cable tension, and (iii) the orientation of the mast with respect to gravity.

Since the first three modes investigated are well separated in frequency, and mode 3 and mode 4 are excited separately, estimation of the modal parameters was carried out with the sdof circle fit technique [23].

Sine sweeps were conducted at forcing amplitudes of approximately 0.1, 0.2 and 0.4 N. The FRFs obtained from the model structure deployed vertically up and prestressed with an active cable tension of 24 N are shown at the end of the paper, in Figs. 9(a), 10(a), 11(a) and 12(a). Nonlinear behaviour is evident: for mode 1, increasing the input amplitude has the effect of increasing mobility, whereas the damping ratio and resonant frequency fall slightly. In contrast, for modes 2, 3 and 4, increasing the input amplitude produces a decrease in mobility, higher damping, and lower resonant frequencies. The variation in modal damping is significant, up to 100% across this range of input amplitudes.

Nonlinear trends in modal behaviour were also observed when testing the structure at different levels of active cable pretension. All modes appeared to become stiffer as the pretension increased. The damping of mode 1 was found to increase for all input levels as the pretension increased, whereas for the higher modes it decreased as the pretension increased. An important difference between mode 1 and the higher modes is in the associated energy dissipation: the measured modal damping for mode 1 lies between 11% and 13%, but only between 1% and 2.5% for the other modes.

Finally, the effects of orientation with respect to gravity were examined by repeating the above tests after fixing the base of the structure to a rigid, vertical wall, and deploying it horizontally. This has the effect of increasing the level of pretension in the passive cables on the upper side of the mast, and of reducing it on the

lower side; the preload in the joints varies accordingly. The behaviour observed was qualitatively similar to that of the structure deployed vertically; the actual damping values were largely unaffected and, overall, there were only slight increases in the resonant frequencies.

4. Component tests

The general trend observed in the experiments is a reduction in frequency, i.e. a softening of the structure, as the excitation amplitude is increased. This behaviour rules out the existence of dead-band mechanisms, i.e. joint free play. Geometric nonlinearity can be excluded as the vibration amplitudes were relatively small. The observed changes in damping and resonant frequencies indicate some form of Coulomb friction nonlinearity. Note that the maximum loss factor for Al-alloy, which is the material used for most parts of the mast, is of the order of 0.1% [24]. This value is far too low to contribute significantly to the modal damping observed experimentally. Friction can occur at the connection between each pantograph rod end and the corresponding end hub, and at the central pivot connecting each rod pair. However, a finite element analysis of the mast, see Section 5, shows that the contact force at the central pivot is small, compared to the forces transmitted through the end hubs. Hence, it is likely that the main source of friction nonlinearity is the pins in the end hubs.

Other possible sources of damping are the active and passive cables. However, damping in the active cable can be neglected, as this cable runs over pulleys mounted on low friction ball bearings and it is almost 20 m long, and hence its strain variation will be very small.

To establish a mathematical model that characterizes these nonlinearities, component level tests were carried out on the two main contributors to the nonlinear behaviour of the structure: the pin joints at the ends of the pantograph rods and the passive cables. The force state mapping method was used to identify their nonlinear behaviour.

4.1. Joints

The pantograph end joints consist of cylindrical pins inserted into rod-end pieces, with a clearance of 0.02 mm. To characterize the behaviour of these joints, an identical steel pin was pushed through a rod end piece and fixed securely to a rigid base. The rod end piece was connected to a 0.6 m length of stranded steel cable, see Fig. 5(a), and the free end of the cable was wound round a tensioning mechanism to control the tension in the cable which, in turn, applied a preload to the pin joint. A lateral excitation force was applied by a shaker attached to the end piece. Force and displacement were measured with a force transducer and laser vibrometer, respectively, and converted to a couple and a rotation. The maximum rotation angle during the tests was less than 0.1°, which is within the predicted range of joint rotations during the vibration tests of the mast. Angular velocities were computed by differentiating the rotations in the frequency domain. Noise effects were removed by applying rectangular windows with a bandwidth of 1 Hz at harmonics of the forcing frequency.

Sinusoidal excitation at 3 Hz was applied, the amplitude being ramped up linearly during the first 20% of the test interval to avoid response transients. Low level random excitation tests had earlier established the system resonance to be about 40 Hz for the lowest preload level tested. Therefore, at 3 Hz the inertia forces can be neglected and hence the measured moments provide a plot of the restoring joint couples. Fig. 6 shows projections of the measured data onto the restoring-couple/rotation plane, for different preloads. In each plot, the ramp-up part of the excitation signal produces a characteristic spiral shape, up to the point where a steady-state condition is reached, corresponding to a repeating hysteresis loop. This behaviour is qualitatively similar to the bilinear loop that is often used in modelling the frictional behaviour of joints [25]. Fig. 7(a) shows such an idealized loop, characterized by an initial linear stiffness, k_1, which suddenly decreases to k_2 once the frictional slip moment, F_r has been reached. The residual stiffness k_2 does not vanish if the joint does not experience complete macro-slip, i.e. for rotations of very small amplitude.

Thus, the pantograph end joints can be characterized by 3 parameters only, whose values are related to the level of preload applied to the joint. These values were estimated by fitting each experimental couple-rotation

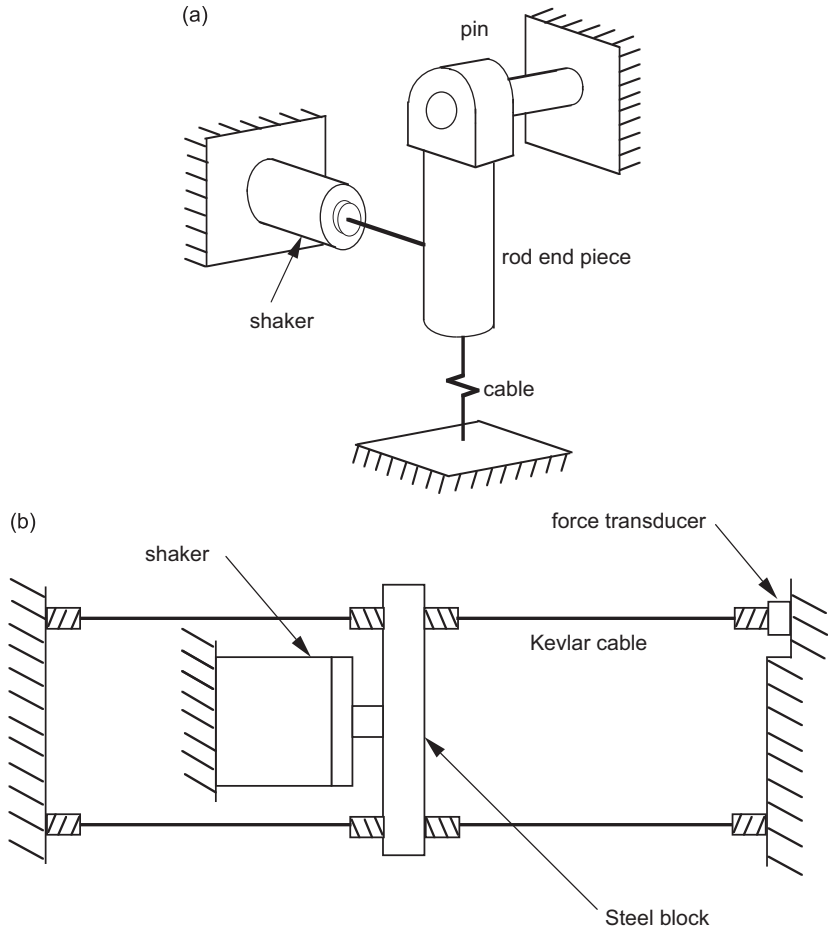

Fig. 5. Schematic diagram of component tests: (a) joint; (b) passive cable.

plot with 4 straight lines, and Fig. 7(b) shows that all 3 parameters vary approximately linearly with the preload.

Fig. 7(c) compares a bilinear hysteresis plot constructed with estimated parameters to the original plot. Although the experimental data does not show the abrupt change of slope that is evident in the regenerated data, the regenerated hysteresis loop is a reasonable fit of the measured data.

4.2. Passive cables

The passive cables are made of straight Kevlar yarns contained in a nylon sheath. The application of a time-varying axial load will induce relative sliding between the yarns and hence some energy dissipation. Higher energy dissipation can be expected in the end connections between the passive cables and the joint hubs. Because the cables function primarily as axial members, the measurement of their axial properties under pretension is of interest. In the absence of an electro-hydraulic shaker, the special set-up shown in Fig. 5(b) was designed and constructed: 4 passive cables are attached to a central steel block, and the opposite ends of these cables are attached to rigid supports. The passive cables are pretensioned by turning the end screws. A shaker is attached directly to the centre of the block. A force transducer mounted on the rigid support monitors the dynamic reaction force in the corresponding cable.

When using this apparatus particular care was taken to ensure that all 4 cables were equally pretensioned and untwisted, since this could change their damping and stiffness properties. Displacements of the steel block were measured by a laser vibrometer. The system was tested at different levels of pretension, ranging from 10

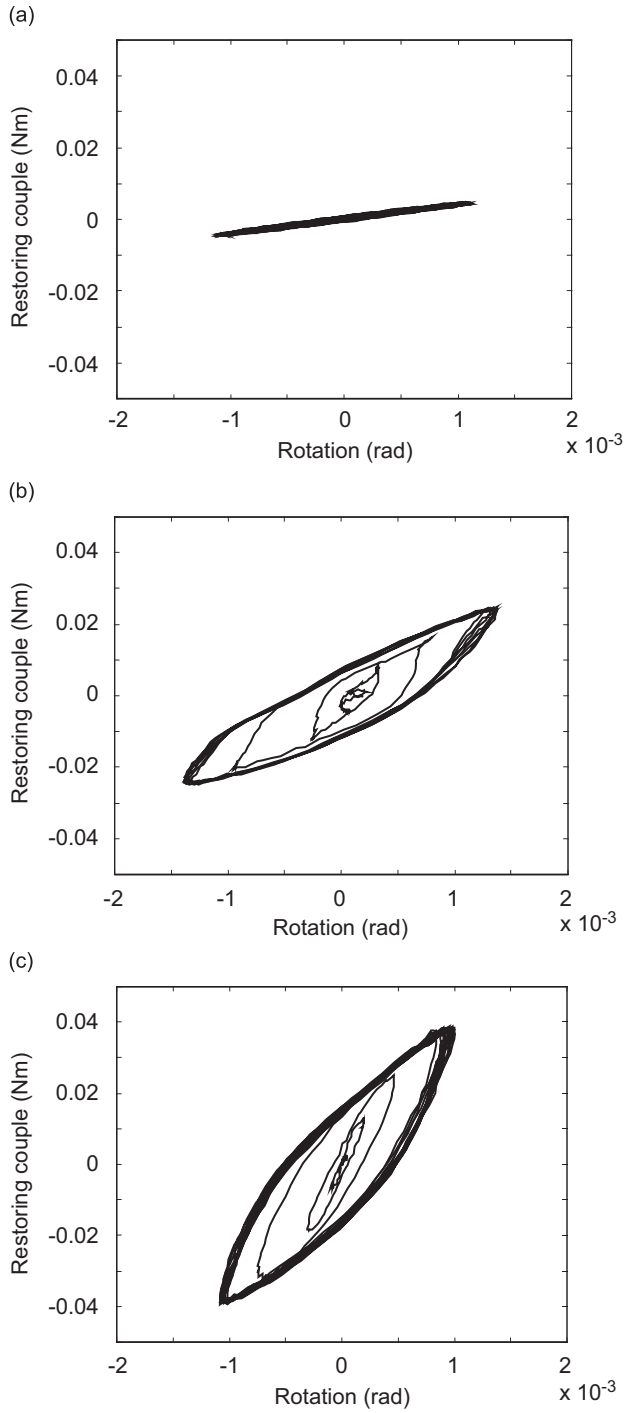

Fig. 6. Restoring couple maps for pantograph joints at different preloads: (a) 15 N; (b) 39 N; (c) 67 N.

to 75 N, and using ramped sine excitation at frequencies from 3 to 70 Hz. The fundamental natural frequency of this system was estimated at 320 Hz, and hence inertia effects could be neglected in setting up the force state map.

Fig. 8(a) is a typical force state map obtained for a pretension of 22 N and an excitation frequency of 6 Hz. This surface is essentially flat, and the appropriate linear stiffness and damping terms were estimated using the

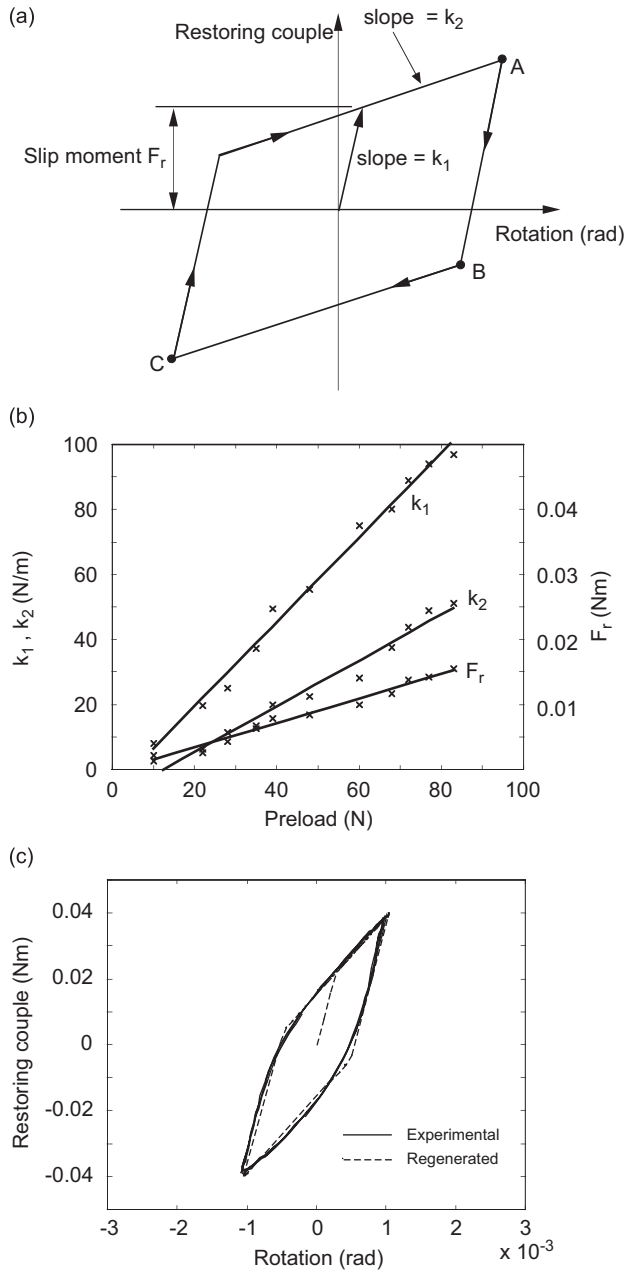

Fig. 7. Relationship between restoring couple and rotation for pantograph joint: (a) simplified relationship; (b) parameter variation with preload; (c) measured and estimated behaviour, for a pretension of 67 N.

method described in Section 1. By repeating this procedure for a wide range of pretensions and excitation frequencies, it was found that the linear stiffness remained relatively constant at approximately 56 kN/m, whereas the linear damping varied as shown in Fig. 8(b). This plot suggests that damping is inversely proportional to both excitation frequency and pretension. A simple function of the type

$$c(\omega, T) = a/\omega^m T^n \tag{12}$$

was chosen, where ω is the excitation frequency and T the cable pretension. The values of a, m, and n were computed by a least squares fit of Eq. (12) to the experimental data, and were found to be 693.5, 1.1, and 0.21, respectively.

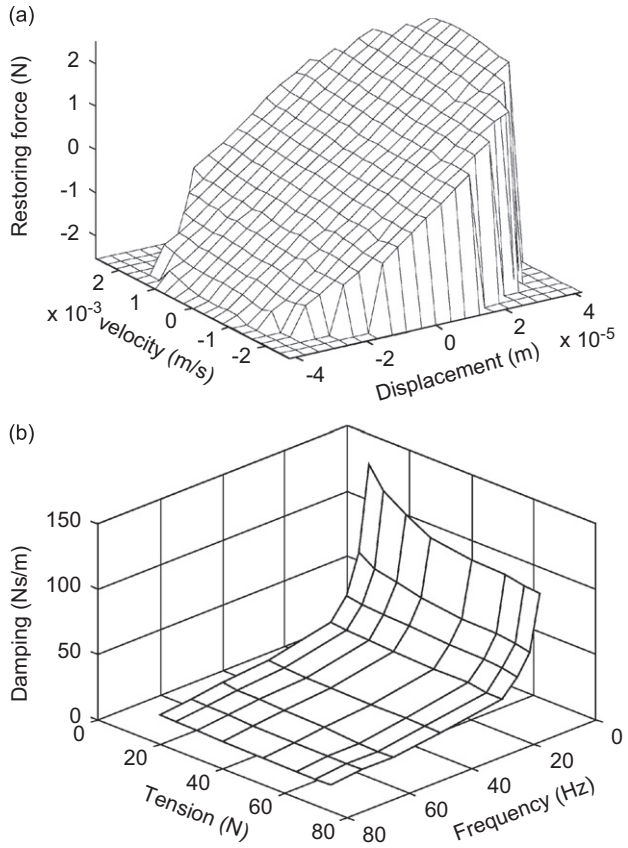

Fig. 8. Measured behaviour of passive cable: (a) force state map for a pretension of 22 N excited at 6 Hz; (b) variation of damping coefficient.

5. Preliminary dynamic modelling

First, a finite-element model of the mast was set up using ABAQUS [26]. The pantograph and passive cables were modelled in ABAQUS with three-dimensional beam elements with cubic displacement shape functions (element B33) and three-dimensional 2-node truss elements with linear displacement shape functions (element T3D2), respectively. A user-defined element was used for the active cable. Its stiffness matrix was calculated from

$$\mathbf{K} = \frac{EA}{L}\mathbf{H}\mathbf{H}^{\mathrm{T}}, \tag{13}$$

where EA is the axial stiffness of the cable and L its total length; $\mathbf{H}$ is the equilibrium matrix [27]. Using this model, the natural frequencies and mode shapes of the model structure were calculated, as well as the state of prestress that is induced by shortening the length of the active cable. A comparison between numerical predictions and the actual state of prestress in the structure showed the measured axial forces to be higher than the predicted values by about 5–10%, due to friction in the joints.

To carry out nonlinear frequency domain simulations, a second model of the mast was developed, using Matlab [28]. The modelling process was essentially similar to that used for the ABAQUS model but, as the mass and stiffness matrices were formulated directly, it was possible to reduce the size of the model, using Guyan reduction [29]. The rotational dofs of the end joints of the pantograph and the translational dofs of the 15 end hub nodes were selected as the master dofs, whereas all other dofs were treated as slave dofs and were condensed out. To assess the quality of the reduced model, a comparison was made between the undamped natural frequencies predicted by the ABAQUS model, the original numerical model, and the reduced model.

Table 1
Natural frequencies (Hz) estimated by different models

Mode	ABAQUS	Matlab (full)	Matlab (reduced)
1st bending	6.002	6.001	6.098
2nd bending	34.06	33.78	33.86
1st axial	58.35	57.76	57.78
1st torsion	62.75	61.18	61.19

Table 2
Predicted variation of natural frequencies (Hz)

Mode	Active cable tension (N)				
	0	11	17	22.6	29.6
1st bending	6.098	5.84	5.76	5.71	5.61
2nd bending	33.86	33.66	33.56	33.49	33.38
1st axial	57.78	57.69	57.65	57.61	57.55
1st torsion	61.19	60.76	60.71	60.30	60.04

Because of the assumptions made in the reduction process, the reduced model does not reproduce exactly the natural frequencies of the original model. However, as can be seen from Table 1, the reduced model produces natural frequencies which are very close to the original model, and also to the ABAQUS model. Due to symmetry, the first two modes have coincident eigenvalues.

The Matlab model was also used to investigate the effects of coupling between the axial force in the pantograph rods and the bending stiffness of the rods. The geometric stiffness matrix was included in the calculation of the natural frequencies of the model structure for different values of the active cable tension; the results are given in Table 2. According to this model, increasing the active cable pretension has the effect of softening the mast, and the reduction in natural frequencies is approximately linear with the active cable tension. However, the experiments had shown the opposite effect and hence it can be concluded that to properly simulate the actual behaviour of the model structure it is necessary to consider the effects of the component nonlinearities on the overall vibration behaviour.

6. Nonlinear dynamic modelling

To obtain the describing function coefficients for the joints of the model structure, the restoring moment-rotation diagram of Fig. 7(a) is divided into two separate response phases. The first phase, corresponding to rotation amplitudes up to F_r/k_1, is linear-elastic. The second, steady-state slip phase, can be modelled by a suitable describing function, assuming a rotation input of the type given in Eq. (1). Because of symmetry, only half of the cycle, ABC, needs to be considered.

The maximum rotation, at point A, corresponds to the phase angle $\psi_A = \pi/2$. From A to B the restoring moment decreases linearly with gradient k_1. At point B

$$\psi_B = \sin^{-1}\left(1 - \frac{2F_r}{k_1\psi_A}\right).$$

Along AB the restoring moment has the expression

$$F_{\mathrm{NL}} = k_1 A \sin\psi - \left[(k_1 - k_2)\psi_A - F_r\left(1 - \frac{k_2}{k_1}\right)\right]. \tag{14}$$

At C the phase angle is $\psi_C = 3\pi/2$, between B and C the restoring moment decreases with gradient k_2, hence

$$F_{\mathrm{NL}} = k_2 A \sin\psi - F_r\left(1 - \frac{k_2}{k_1}\right). \tag{15}$$

The equivalent stiffness and damping can be derived by substituting Eqs. (14) and (15) into Eqs. (8) and (9), changing the lower and upper integration limits to $\pi/2$ and $3\pi/2$, respectively, and multiplying by 2.

For the initial, linear phase $\psi_A < F_r/k_1$ and

$$k_{\text{eq}} = k_1, \tag{16}$$

$$c_{\text{eq}} = 0. \tag{17}$$

Once $\psi_A \geqslant F_r/k_1$, the macro-slip phase has

$$k_{\text{eq}} = \frac{(k_1 - k_2)}{\pi}[\psi_B + (1-\delta)\sqrt{\delta(2-\delta)}] - \frac{k_1 - 3k_2}{2}, \tag{18}$$

$$c_{\text{eq}} = \frac{4F_r(k_1 - k_2)}{\pi\omega k_1^2 A^2}(k_1\psi_A - F_r), \tag{19}$$

where

$$\delta = \frac{2F_r}{k_1\psi_A}$$

and k_1, k_2, and F_r are related to the preload as shown in Fig. 7(b).

The describing function coefficients, obtained in Section 4.2, are $k_{\text{eq}} = 56\,\text{kN/m}$ and $c_{\text{eq}} = 693.5/\omega^{1.1}T^{0.21}\,\text{Ns/m}$.

To calculate the dynamic response of the mast, the mode-superposition method is used. The equations of motion are best written in the frequency domain, as follows:

$$[-\omega^2\mathbf{M} + \mathrm{j}\omega\mathbf{C}_{\text{eq}} + (\mathbf{K} + \mathbf{K}_{\text{eq}})]\mathbf{y} = \mathbf{F}, \tag{20}$$

where $\mathbf{M}$ and $\mathbf{K}$ are the standard, linear mass and stiffness matrices, respectively. $\mathbf{K}_{\text{eq}}$ and $\mathbf{C}_{\text{eq}}$ are the amplitude and frequency-dependent equivalent stiffness and damping matrices, respectively, containing the describing function coefficients for the joints and the passive cables.

To reduce the size of the problem, a standard modal truncation technique is employed. Eq. (20) is transformed to a set of reduced modal coordinates $\mathbf{q}$, where $\mathbf{y} = \boldsymbol{\Phi}_m\mathbf{q}$

$$[-\omega^2\mathbf{M}^* + \mathrm{j}\omega\mathbf{C}^*_{\text{eq}} + (\mathbf{K}^* + \mathbf{K}^*_{\text{eq}})]\mathbf{q} = \mathbf{F}^*. \tag{21}$$

The reduced matrices $\mathbf{M}^* = \boldsymbol{\Phi}_m^{\mathrm{T}}\mathbf{M}\boldsymbol{\Phi}_m$ and $\mathbf{K}^* = \boldsymbol{\Phi}_m^{\mathrm{T}}\mathbf{K}\boldsymbol{\Phi}_m$, and the reduced force vector $\mathbf{F}^* = \boldsymbol{\Phi}_m^{\mathrm{T}}\mathbf{F}$ are computed only once. However $\mathbf{K}^*_{\text{eq}} = \boldsymbol{\Phi}_m^{\mathrm{T}}\mathbf{K}_{\text{eq}}\boldsymbol{\Phi}_m$ and $\mathbf{C}^*_{\text{eq}} = \boldsymbol{\Phi}_m^{\mathrm{T}}\mathbf{C}_{\text{eq}}\boldsymbol{\Phi}_m$ still need to be re-computed at each iteration, as their coefficients vary with frequency and amplitude.

The following procedure is adopted to ensure accurate modelling of the nonlinear behaviour of the structure during a frequency sweep at a particular force level. Initially, the eigenvectors of the linear non-dissipative model are used to carry out a first modal reduction. Then, having determined an initial estimate of the response amplitude, $\mathbf{K}_{\text{eq}}$ and $\mathbf{C}_{\text{eq}}$ are computed. This computation requires knowledge of the axial preload in all members, determined by means of the linear ABAQUS model. Then, updated eigenvectors are computed from the eigenvalue problem

$$-\omega^2\mathbf{M}\mathbf{y} = \mathbf{K} + \mathbf{K}_{\text{eq}}\mathbf{y} \tag{22}$$

and a new modal reduction is carried out using the updated eigenvectors. Eq. (21) is solved iteratively until convergence is achieved, at which point the frequency is incremented and the iteration repeated. At some point it may be necessary to determine updated eigenvectors, if $\mathbf{K}_{\text{eq}}$ changes substantially, due to changes in response amplitudes and/or the excitation frequency. However, since the equivalent stiffness is not dependent on frequency, if the response amplitude does not change significantly, as in a narrow band sweep near resonance, then the updated modal matrices need only be computed at the start frequency.

A way of ensuring consistent results is to test for convergence as follows. First, the modal matrices are updated only once, at the start frequency. Next, the matrices are updated twice, at the start frequency and also in the middle of the frequency sweep. The results from the two runs are then compared and, if the difference between the two sets of results does not exceed a specified tolerance, then convergence has been achieved.

If not, a third analysis is carried out, with the modal matrices updated three times within the frequency sweep, and so on, until convergence is achieved.

The simulations presented in this paper required no more than three analyses. Also, the iterative reduced model described above, including 5 modal coordinates, run over 300 times faster than a full nonlinear simulation.

7. Nonlinear modal predictions

To simulate the dynamic response of the mast, FRFs of the model structure were computed according to the force amplitudes, active cable pretension and orientation with respect to gravity. Ten modal dofs were included in the analysis, and the iterative solution of Eq. (21) was carried out using NAG Fortran subroutine C05NCF [30]. Figs. 9(b), 10(b), 11(b) and 12(b) show the simulated response of a vertically deployed mast, near the first four resonant frequencies. Resonant frequencies and modal damping estimates for these modes are given in Table 3and compared with experimental results.

For mode 1, the numerical simulations in Fig. 9(b) have predicted the effects of increasing damping and resonant frequencies with increasing force amplitude that were observed in the experiments, Fig. 9(a). The resonant frequencies are within 4% of the measurements, however the simulations have clearly under-predicted the overall damping levels, resulting in much larger FRF amplitudes. Note that the vertical scales in the two figures are not the same. The predicted modal damping is between 60% and 70% lower than measured.

A careful examination of the model structure showed that the joint hubs at the top of the mast are free to undergo small amplitude rotations about the end pins. So, even small eccentricities in the dynamic excitation applied to these joints result in unmodelled energy dissipation effects. To remove this effect, the top bay of the

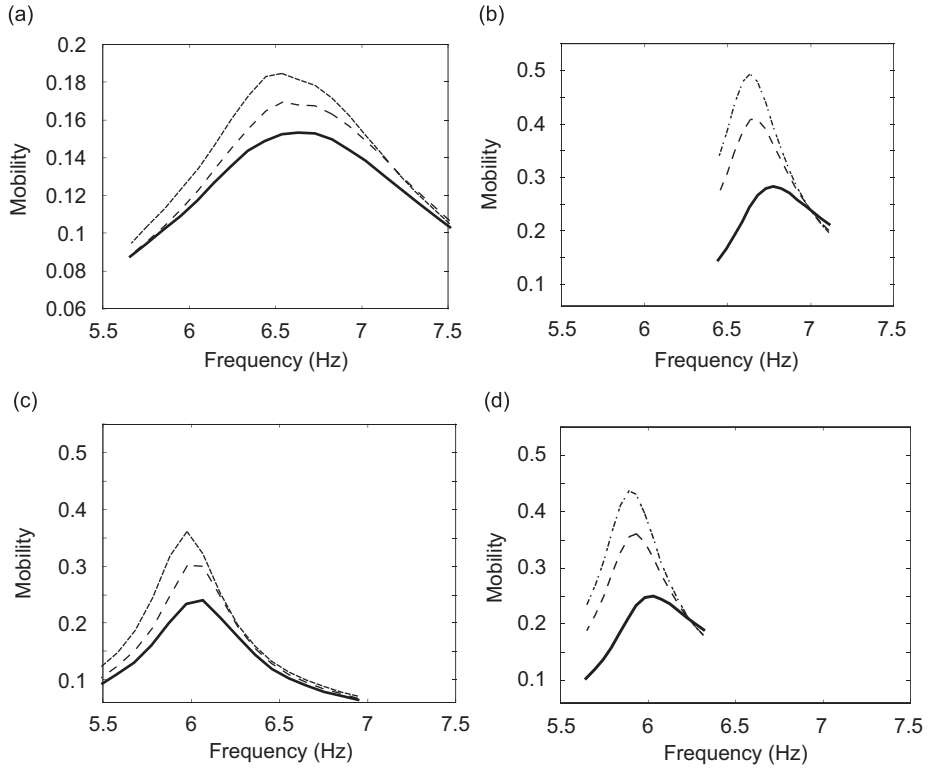

Fig. 9. FRFs for mode 1 (first bending) for active cable pretension of 24 N: (a) experiment; (b) simulation; (c) experiment (stiffened mast); (d) simulation (stiffened mast). Excitation amplitudes: solid lines 0.1 N, dashed lines 0.2 N, dot–dash lines 0.4 N.

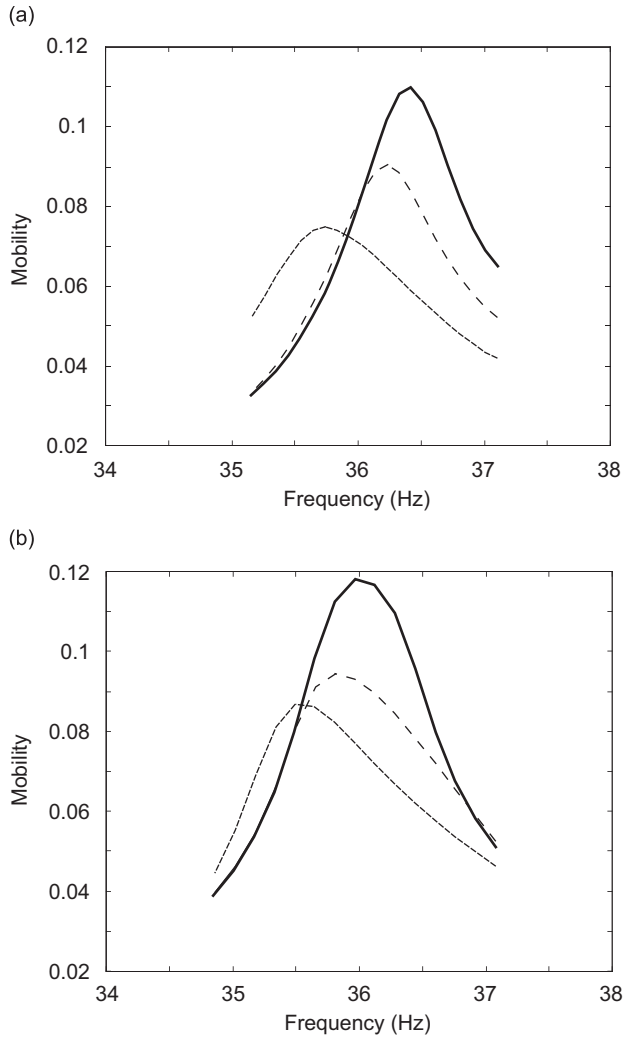

Fig. 10. FRFs for mode 2 (second bending): (a) experiment; (b) simulation. See caption of Fig. 9.

mast was stiffened by adding a lightweight triangular frame and a new set of narrow band of sine sweeps were carried out. Fig. 9(c,d) compares the FRFs obtained from the new set of modal tests with predictions from the modified numerical model; more detailed results are given in Table 3. Note that now the agreement between experiment and simulation is excellent. Also note that the frequency of the first mode has decreased, due to the mass of the stiffening frame.

For modes 2, 3 and 4 the simulations—see Figs. 10(b), 11(b), and 12(b)—have been able to capture the trends in damping and resonant frequency. As the force amplitude is increased, the resonant frequency decreases and the modal damping increases. A comparison of the modal parameters obtained from the simulations against the experimental data, Table 3, shows very good agreement. For the frequencies the error is less than 1.5%. For mode 2, the modal damping for the low and medium excitation amplitudes is overestimated in the simulations, while the modal damping under high-excitation amplitudes is slightly underestimated. The average discrepancy is 16.5%. For mode 3, the downward shift in resonant frequency with increasing force amplitude is not as pronounced in the numerical simulations as in the experiments. The modal damping is predicted to within 11% of the measured value. For mode 4, the error in the prediction of resonant frequency is less than 1%, but the frequency shift with force amplitude and the associated damping are underestimated. Further tests [31] have shown that when the pretension level is increased the level of

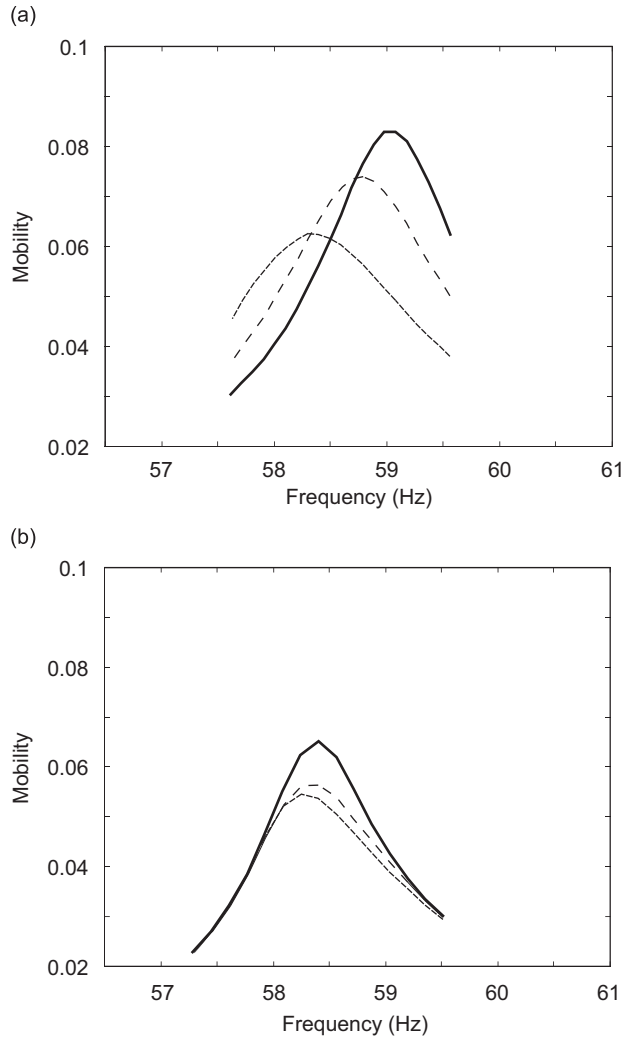

Fig. 11. FRFs for mode 3 (first axial); (a) experiment; (b) simulation. See caption of Fig. 9.

damping decreases, and the accuracy of the simulation improves considerably. It is thought that this effect may be due to micro-slip along the direction of the pin, which has not been modelled.

The variation in resonant frequency and modal damping with the level of active cable pretensions were also systematically investigated by experiment and simulation. It was found that when the active cable tension is increased the resonant frequencies increase, the modal damping decreases, and the FRF amplitudes become correspondingly larger.

The drop in modal damping is caused by the passive cables, whose effects are more significant than the damping from the pin joints.

8. Discussion and conclusion

A special feature of cable-stiffened pantographic deployable structures is that after deployment they are subjected to an overall state of prestress, which pretensions all of the cables and thus increases the stiffness of the pantograph.

It has been shown in this paper that an indirect effect of this overall state of prestress is to considerably increase stiffness and friction at the end joints of the pantograph rods. Under dynamic excitation of sufficiently

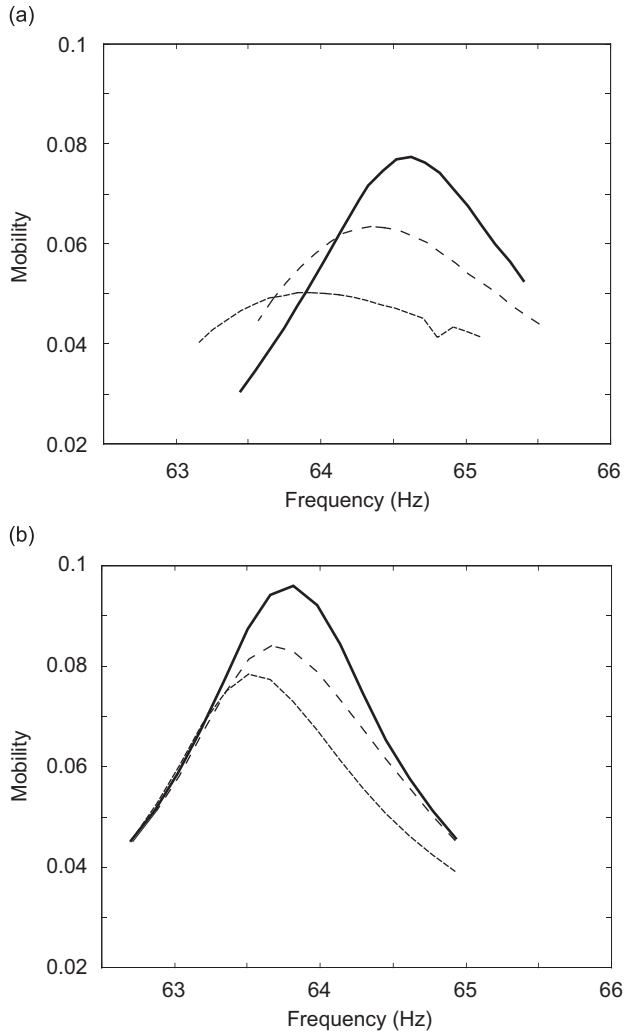

Fig. 12. FRFs for mode 4 (first torsional): (a) experiment; (b) simulation. See caption of Fig. 9.

large amplitude micro-slip begins between the journal bearings and the internal pins, thus partially releasing the rotational dof at the ends of each rod. Over a complete, small amplitude vibration cycle the moment–rotation relationship for each joint forms a characteristic hysteresis loop, which is a function of the joint preload, with associated amplitude-dependent and frequency-dependent stiffness and damping. It has also been shown that another major source of energy dissipation is the behaviour of the passive cables, made of Kevlar. Their damping decreases as the cable preload and the excitation frequency are increased. Both effects have been accurately characterized using the restoring force identification method. Studies of other types of deployable structures have often been plagued by chaotic behaviour in the joint response, but in the case of cable-stiffened pantographic structures this is not a problem because joint gaps are removed, in effect, by the preload.

The present study has shown the importance of including dynamic effects in characterizing component nonlinearities. In addition to assessing the effects of prestress levels, it is necessary to test the component at different frequencies (where possible, covering the frequency range of interest) to fully assess any frequency-dependent behaviour.

A particular model structure has been investigated in detail. It has been found that the resonant frequencies of its first 4 modes tend to decrease when the excitation amplitude is increased. Modal damping is usually in the range 1–5% for all 4 modes and tends to increase with the excitation amplitude for some modes, but to

Table 3
Modal parameters

Mode	Excitation amplitude	Experiment		Simulation	
		f (Hz)	ζ	f (Hz)	ζ
1	Low	6.63	0.121	6.66	0.048
	Medium	6.61	0.115	6.63	0.036
	High	6.59	0.115	6.62	0.034
1 (modified)	Low	6.03	0.049	5.91	0.042
	Medium	6.01	0.041	5.89	0.037
	High	5.96	0.033	5.87	0.036
2	Low	36.22	0.013	35.93	0.015
	Medium	36.05	0.014	35.58	0.018
	High	35.66	0.022	35.29	0.019
3	Low	58.96	0.010	58.33	0.010
	Medium	58.74	0.013	58.14	0.012
	High	58.36	0.015	58.09	0.014
4	Low	64.58	0.011	63.74	0.010
	Medium	64.10	0.015	63.55	0.012
	High	63.72	0.020	63.44	0.013

decrease for other modes. This is a typical feature of systems subject to dry friction, whose damping for increasing response amplitudes initially increases but then starts to decrease when gross slip begins. A nonlinear dynamic model of this structure has been set up, which accounts for the effects of joint preload and passive cable pretension via the equivalent stiffness and damping coefficients discussed above. The equations of motion of the structure, which contain frequency-dependent and amplitude-dependent terms, are solved iteratively. It has been shown that this model predicts accurately the resonant frequencies of the first 4 modes of the structure. It also predicts modal damping to good accuracy, provided that unmodelled dofs, such as joint rocking, are not excited.

Extending this approach to the prediction of the in-orbit behaviour of cable-stiffened pantographic deployable structures should not pose any difficulties, as only component level tests are required. Such tests can be carried out in small vacuum chambers, without the need for a large facility. Also, it will be possible to remove gravity effects from computer models that have been initially validated against the results of tests carried out in a gravity environment.

Finally, it is well known that structures with tightly clamped joints, such as erectable structures, have very low levels of damping, which raises stability issues for active vibration control. Deployable structures which contain pin joints have higher damping, which can be tuned by varying the level of prestress. It is also possible to vary the stiffness of the structure by increasing the prestress level up to the point where the joints start behaving as fully clamped.

Acknowledgments

The research presented in this paper was carried out in the Department of Engineering, University of Cambridge. Technical assistance from the Workshops of the Engineering Department is gratefully acknowledged.

References

[1] M.M. Mikulas, M. Thomson, State of the art and technology needs for large space structures, in: A.K. Noor, S.L. Venneri (Eds.), *Flight-Vehicle Materials, Structures, and Dynamics—Assessment and Future Directions*, Vol. 1, ASME, New York, 1994, pp. 173–238.
[2] S. Pellegrino, Large retractable appendages in space, *Journal of Spacecraft and Rockets* 32 (1) (1995) 127–142.

[3] B. Hanks, L. Pinson, Large space structures raise testing challenges, *Astronautics and Aeronautics* 21 (10) (1983) 34–53.
[4] C.A. Rogers, W.L. Stutzman, T.G. Campbell, J.M. Hedgepeth, Technology assessment and development of large deployable antennas, *ASCE Journal of Aerospace Engineering* 6 (1) (1993) 34–54.
[5] Z. You, S. Pellegrino, Cable-stiffened pantographic deployable structures: part 1—triangular mast, *AIAA Journal* 34 (4) (1996) 813–820.
[6] Z. You, S. Pellegrino, Cable-stiffened pantographic deployable structures: part 2: mesh reflector, *AIAA Journal* 35 (8) (1997) 1348–1355.
[7] A. Gelb, W. Van der Welde, *Multiple-Input Describing Functions and Nonlinear System Design*, McGraw-Hill, New York, 1968.
[8] M. Bowden, J. Dugundji, Joint damping and nonlinearity in dynamics of space structures, *AIAA Journal* 28 (4) (1990) 740–749.
[9] J. Chapman, F. Shaw, W. Russell, Nonlinear transient analysis of joint dominated structures, *AIAA Paper 87-0892*, 1987.
[10] J. Onoda, T. Sano, K. Minesugi, Passive damping of truss vibration using preloaded joint backlash, *AIAA Journal* 33 (7) (1995) 1335–1341.
[11] R. Ikegami, S. Church, D. Keinholz, B. Fowler, Experimental characterization of deployable trusses and joints, *Proceedings of the NASA Workshop on Structural Dynamics and Control Interaction of Flexible Structures*, Huntsville AL, USA, 1986, pp. 1271–1287.
[12] F. Moon, G. Li, Experimental study of chaotic vibrations in a pin-jointed space truss structure, *AIAA Journal* 28 (5) (1988) 915–921.
[13] J. Hinkle, L. Peterson, Experimental dynamic characterization of a reconfigurable adaptive precision truss, *Proceedings of the 35th AIAA/ASME/ASCE/AHS/ASC Structures, Structural Dynamics and Materials Conference*, Hilton Head SC, USA, 1990, pp. 740–749 (AIAA Paper 94-1734).
[14] E.F. Crawley, A. Aubert, Identification of nonlinear structural elements by force-state mapping, *AIAA Journal* 24 (1) (1986) 155–162.
[15] G.E.B. Tan, S. Pellegrino, Non-linear dynamic identification: an application to prestressed cable structures, *Journal of Sound and Vibration* 208 (1) (1997) 33–45.
[16] E.F. Crawley, M. Barlow, M. Van Schoor, A. Bicos, Variation in the modal parameters of space structures, *Proceedings of the 33rd AIAA/ASME/ASACE/AHS/ASC Structures, Structural Dynamics and Materials Conference*, Dallas TX, USA, 1992, pp. 1212–1228.
[17] B. Masters, E.F. Crawley, Multiple degree-of-freedom force state component identification, *AIAA Journal* 32 (11) (1994) 2276–2285.
[18] B. Masters, E.F. Crawley, Multiple degree of freedom force state component identification, MIT Space Engineering Research Center, SERC1-94, 1994.
[19] S.L. Folkman, A. Edwin, D. Greg, Influence of pinned joints on damping and dynamic behaviour of a truss, *Journal of Guidance, Control and Dynamics* 18 (6) (1995) 1398–1403.
[20] J.G. Bingham, S.L. Folkman, Measured influence of gravity on the dynamic behaviour of a truss using pinned joints, *Proceedings of the 37th AIAA/ASME/ASCE/AHS/ASC Structures, Structural Dynamics and Materials Conference*, Salt Lake City UT, USA, 1996, pp. 1043–1053 (AIAA Paper 96-1437).
[21] B.D. Ferney, S.L. Folkman, Results of force-state mapping tests to characterize struts using pinned joints, *Proceedings of the 36th AIAA/ASME/ASCE/AHS/ASC Structures, Structural Dynamics and Materials Conference*, New Orleans LA, USA, 1995, pp. 2217–2225 (AIAA Paper 95-1150).
[22] F. Deblauwe, D. Brown, R.J. Allemang, The polyreference time domain technique, *Proceedings of the 5th International Modal Analysis Conference*, London, UK, 1987, pp. 832–845.
[23] D.J. Ewins, *Modal Testing: Theory and Practice*, second ed., Research Studies Press, Baldock, UK, 2000.
[24] B. Lazan, *Damping in Materials and Members in Structural Mechanics*, Pergamon Press, Oxford, UK, 1968.
[25] C.H. Menq, J.H. Griffin, Comparison of transient and steady state finite element analyses of the forced response of a frictionally damped beam, *Journal of Vibration, Acoustics, Stress, and Reliability in Design* 107 (1) (1985) 19–25.
[26] Hibbit, Karlsson and Sorensen, *ABAQUS Version 5.4*, Pawtucket, 1994.
[27] A.S.K. Kwan, S. Pellegrino, Matrix formulation of macro-elements for deployable structures, *Computers and Structures* 50 (2) (1994) 237–254.
[28] Mathworks, *MATLAB Version 4.2*, Natick, MA, 1995.
[29] R.R. Craig, *Structural Dynamics—An Introduction to Computer Methods*, Wiley, London, UK, 1994.
[30] Numerical Algorithm Group, *Fortran Library Mark 14*, Oxford, 1990.
[31] G.E.B. Tan, Non-Linear Vibration of Cable-deployed Space Structures, PhD Dissertation, University of Cambridge, 1997.